



Multiplex integrated cavity output spectroscopy of cold PAH cations

Ludovic Biennier ^{a,*}, Farid Salama ^a, Manish Gupta ^b, Anthony O’Keefe ^b

^a NASA Ames Research Center, Space Science Division, Mail Stop 245-6, Moffett Field, CA 94035-1000, USA

^b Los Gatos Research, 67 East Evelyn Ave., Suite 3, Mountain View, CA 94041, USA

Received 25 October 2003; in final form 30 January 2004

Published online: 5 March 2004

Abstract

Multiplex Integrated Cavity Output Spectroscopy (MICOS) is a new cavity-enhanced absorption method that allows the use of broadband dye nanosecond pulsed laser sources and offers a sensitivity equivalent to CRDS. MICOS has been coupled to a pulsed discharge slit nozzle to measure the spectra of the cold naphthalene ($C_{10}H_8^+$), acenaphthene ($C_{12}H_{10}^+$) and pyrene ($C_{16}H_{10}^+$) cations in the gas phase. A femtosecond relaxation timescale is measured for the $D_5 \leftarrow D_0$ (0–0) transition of $C_{16}H_{10}^+$. Spectra recorded at high plasma energies also show evidence of fragmentation. The CH radical is observed and carbon nanoparticles are generated in the plasma.

Published by Elsevier B.V.

1. Introduction

Polycyclic Aromatic Hydrocarbons (PAHs) are an important component of interstellar dust and are found in meteorites and interplanetary dust particles. PAHs are thought to carry the infrared emission bands (UIBs) that are detected in a wide variety of galactic and extragalactic environments [1]. PAHs are also thought to carry some of the diffuse interstellar bands (DIBs) seen in absorption in the near ultraviolet to near infrared spectra of stars that are obscured by diffuse interstellar clouds [2,3]. Interstellar PAHs can be neutral or ionized depending on the environmental conditions (density and radiation field). In the diffuse interstellar medium, however, PAHs are expected to be primarily present as free, cold, molecular ions [4]. The identification of the carriers of the DIBs has important implications for our understanding of the evolution of the interstellar medium and this issue has motivated an extensive laboratory effort over the past decade (for a recent review see [5]). New insights in the electronic [6–9] and vibrational [10, 11] spectroscopy and the intramolecular dynamics of free PAH ions have

recently been gained through the application of state-of-the-art laser-based techniques specifically developed to address this challenging problem.

Here, we describe a new technique, Multiplex Integrated Cavity Output Spectroscopy (MICOS) that we have developed to measure the absorption spectrum of free, cold, large carbon-bearing molecular ions and discuss the new results that have been obtained with this method. In our previous studies [7], we followed an approach based on Cavity Ring Down Spectroscopy (CRDS). CRDS is a *time-domain* method which monitors the time dependence of photons escaping the cavity after their injection in the cavity mode(s). The high sensitivity of cavity-based methods rests upon the long residence time of the photons trapped inside the high finesse cavity. Recently, *intensity-domain* methods exploiting high finesse cavities have been introduced: Cavity Enhanced Absorption Spectroscopy (CEAS) and Integrated Cavity Output Spectroscopy (ICOS) [12,13].

A number of groups [14,15] have also taken advantage of the use of a broadband source for injection of photons in a high finesse cavity. We have adopted yet another approach, and developed a MICOS spectrometer that uses a broadband nanosecond pulsed dye laser that is robust (a crucial requirement when coupled to a pulsed discharge nozzle that is a recognized source of

* Corresponding author. Fax: +33-2-23-23-61-90.

E-mail address: ludovic.biennier@univ-rennes1.fr (L. Biennier).

noise and instability), simple to setup and to operate, and of moderate cost. Our technique combines the ICOS detection scheme with the use of a spectrally broad light source. In this design, the output of the cavity is sent through a wavelength dispersing element (such as a grating) to a linear CCD detector array. The operating principle of this method was first demonstrated with Ringdown Spectral Photography by measuring the weak oxygen b–X (1–0) band [16]. In our implementation, the broadband dye laser output coupler is absent and the light is thus generated after only two passes in the active medium. This optical configuration results in a *modeless* laser emission. Although the broadband amplified spontaneous emission spectrum is structured, it was found that these structures are stable over time and can be removed by dividing two consecutive spectra.

In this Letter, we report direct absorption measurements in the gas phase of the electronic bands of the cold naphthalene ($C_{10}H_8^+$), acenaphthene ($C_{12}H_{10}^+$) and pyrene ($C_{16}H_{10}^+$) cations and describe the method developed for this specific purpose. The MICOS spectrometer is described in Section 2. The results are discussed in the following section where they are compared with CRDS measurements. The conclusions are discussed in Section 4.

2. Experimental

The experimental apparatus combines a pulsed discharge slit nozzle (PDN) for the production of free, cold

aromatic ions with a MICOS spectrometer for the detection and the measurement of the spectra of these ions. The PDN component of the experimental system has been modified from the original design of Saykally et al. [17] and is described in detail in [7]. Fig. 1 shows a schematic of the experimental setup. Briefly, in our typical running conditions (1 atm backing pressure of Argon, <1% PAH dilution) the PDN source produces very intense, 500 μ s-long, ionized gas pulses every 100 ms. The plasma expansion generated by the PDN is probed by the spectrometer about 2 mm downstream the electrodes. The photon source is a broadband home-made dye laser. The pump beam generated by the second/third harmonic of a nanosecond pulsed Nd:YAG laser (Spectra Physics GCR-130 with 6350 injection seeder, 210 mJ at 532 nm and 100 mJ at 355 nm) is focused into the dye cell with a cylindrical lens. The dye laser consists of one 40-mm long side-pumped dye cuvette and one back mirror (Lambda Physik). The output coupler is removed from the dye laser cavity because it induces strong (\sim 15% amplitude) periodic modulations of the spectrum of the laser. As a consequence, light is generated after only two passes in the active medium by amplified spontaneous emission precluding the emergence of a dye laser modes comb. The output characteristics of this modeless laser are intermediate between a truly coherent laser oscillator and a completely incoherent thermal source. Dye solutions of a mixture of DCM (\sim 450 mg/l dissolved in DMSO) and of Coumarin 440 (\sim 300 mg/l in methanol) were prepared for the 640–680 nm and the 425–465 nm spectral regions, respec-

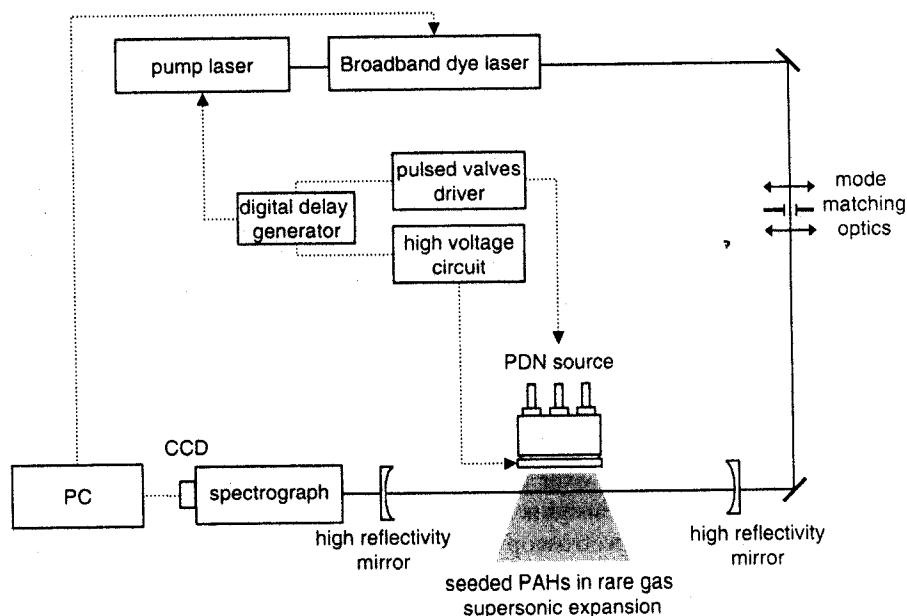


Fig. 1. MICOS-PDN experimental setup. The MICOS spectrometer relies on a broadband dye laser combined to a high finesse cavity, $\mathcal{F} \leq 20000$, and a medium resolution spectrograph. The optical configuration of the dye laser consists in one back mirror and a side-pumped dye cuvette, resulting in a modeless broadband emission.

tively. For pump energy above ~ 100 mJ, the conversion efficiency is about 5%. The divergence of the output beam is ~ 4.2 mrad. The energy coupled into the cavity is typically ~ 1 μ J (spread over 20 nm at half maximum) equivalent to a number of photons in the $4\text{--}7 \times 10^{12}$ range depending on the wavelength window. The beam is collimated to maximize the throughput of the cavity. The cavity output mode pattern is imaged using a progressive scan high resolution camera (PULNIX TM-1300) and a 8-bit frame grabber (PIXCI SV5) looking through the rear mirror of the cavity. The photons leaking out the cavity are collected by a 68 mm spectrograph (Ocean Optics USB2000) in a Czerny–Turner configuration. The spectrograph is equipped with a 50 μ m entrance slit, a 1200 grooves/mm holographic grating and a 2048 pixels linear CCD array with a 12-bit A/D vertical resolution (Sony ILX511) that allows to cover the whole 400–700 nm range with a typical 0.75 nm resolution. The acquisition is triggered by a digital delay generator (SRS DG535) and the collection time set to its minimum value of 50 μ s. The data is transferred through a Universal Serial Bus to the PC for treatment by commercial software (Ocean Optics, OOIBase32). The signal collected on the CCD array, and displayed in Fig. 2, usually shows some asymmetry as the spectral profile corresponds to the convolution of the dye gain curve with the transmission curve of the high reflectivity mirrors – and marginally with the response curve of the spectrograph. The treatment of the signal is performed in three steps. First a reference jet spectrum (R) is recorded that consists of 1000 averaged single beam spectra with the gas jet pulse expanding and the plasma off. A sample spectrum (S) is then recorded over the same duration with the plasma turned on. The absorbance spectrum (A) is finally retrieved by dividing the sample spectrum (S) by the reference spectrum (R). Note that a dark spectrum (D) is subtracted from both the reference and sample spectra.

In addition to shot to shot cavity-input power fluctuations ($\sim 10\%$) exemplified on Fig. 2a, each single beam spectrum shows noise at the three CCD counts level ($\leq 0.3\%$ of the peak envelope) that can be reduced by averaging (Fig. 2b). Possible sources of noise are inhomogeneities of the dye gain and seeding photon noise. The latter phenomenon arises from the statistical nature of the spontaneous emission of photons from excited levels. Noise cancellation is obtained after averaging 1000 spectra leading to an absorbance noise level below 0.1%. This value translates into 0.1 ppm/pass for typical 100 ppm/pass high reflectivity mirrors or 5.75×10^{-8} cm/ $\sqrt{\text{Hz}}$ for a $l = 55$ cm long cavity. To account for multiplexing, the detection limit is divided by the square root of the number of spectral elements that are sampled simultaneously. A spectral element (active detector), defined by the extent of the coverage of the image of the slit on the grating, is about 6.5 pixels

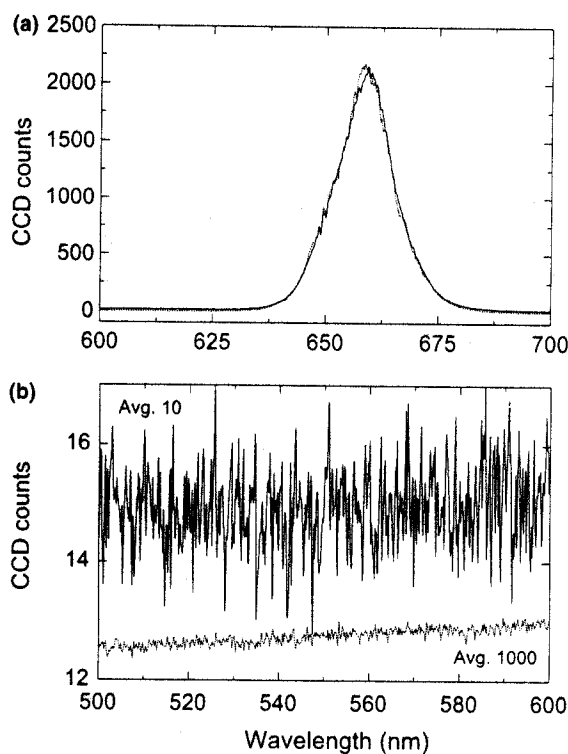


Fig. 2. Cavity output spectra of the broadband dye (DCM diluted in DMSO) pulse with the plasma turned off. Displays result from the averaging of 10 (full line) and 1000 (dotted line) single beam spectra. (a) The spectral profile corresponds to the convolution of the dye gain curve with the transmission curve of the high reflectivity mirrors and with the response curve of the spectrograph. The output is affected by shot-to-shot power fluctuations ($\sim 10\%$). (b) Close up of the off-peak region of the cavity output spectrum. Top and bottom traces, slightly shifted for convenience, show standard deviation of 1.05 and 0.108, respectively. Note: a high quality dark spectrum has been subtracted from all spectra shown here.

under the current design. This leads to an estimated detection limit of 3.2×10^{-9} cm/ $\sqrt{\text{Hz}}$, a value that is about one order of magnitude higher than the CRDS detection limit measured under similar conditions. MICOS is, however, much less affected by the long term fluctuations of the PDN source as all spectral data points are recorded simultaneously. Moreover, our experimental studies show that it is extremely difficult to achieve detection limits better than 0.1 ppm/pass with either of those two techniques when coupled to a PDN plasma source. The spectra are calibrated using Xe and Ne emission lines (Oriel calibration lamps 6033 for Xe and 6032 for Ne) placed before the entrance cavity mirror to ensure the same light path. In contrast to CRDS, MICOS is not an absolute measurement method. The absorption scale can be either inferred from the mirror reflectivity curve (when available) or calibrated using previously recorded CRDS spectra of the empty cavity. For example, if the losses of the empty cavity are of the order of 100 ppm/pass, a 1% absorbance spectral feature will correspond to a ~ 1 ppm/pass absorption in a first approximation. To be valid, this calibration

procedure requires that measurements be performed under very similar conditions with the two techniques.

3. Results and discussion

The electronic absorption spectra of gas-phase naphthalene ($C_{10}H_8^+$), acenaphthene ($C_{12}H_{10}^+$) and pyrene ($C_{16}H_{10}^+$) cations were measured with the MICOS technique. The $D_2 \leftarrow D_0$ (0–0) and (1–0) vibronic bands of the naphthalene cation and the $D_2 \leftarrow D_0$ (0–0) vibronic band of the acenaphthene cation are reported in Sections 3.1 and 3.2, respectively. These first two PAH cations were chosen because detailed CRDS data are available for comparison with the MICOS data [7]. The gas-phase spectrum of the $D_5 \leftarrow D_0$ (0–0) band of the pyrene cation is reported for the first time and is discussed in Section 3.3. Evidence for fragmentation and soot formation is also seen at higher discharge energies through the observation of the (A–X) (0–0) CH radical absorption band and the detection of carbon nanoparticles in the PDN source. These results will be discussed separately [18].

3.1. The naphthalene cation ($C_{10}H_8^+$)

Naphthalene was initially selected in this work because it is a prototype for linear PAHs. The first two absorption bands of the vibrational progression of the ${}^2B_{3g}(D_2) \leftarrow X^2A_u(D_0)$ electronic band system of the naphthalene cation (Np^+) were measured at 670.7 and 648.9 nm, respectively. The widths of the two bands before deconvolution, which include the contribution of the complexes formed with argon atoms, are 1.5 nm in both cases. The MICOS spectrum of Np^+ , displayed in Fig. 3a, is well reproduced by the convolution of the synthetic spectra of Np^+ , Np^+-Ar and Np^+-Ar_2 (in the 20:6:1 ratio derived from the CRDS spectra) with the apparatus function ($\delta v_{app} \sim 0.75$ nm FWHM Gaussian lineshape). When accounting for extra losses, one can derive the absolute absorption intensity at each wavelength. By following this procedure, the maximum absorption values are found to be 33 and 14 ppm/pass for the (0–0) and (1–0) vibronic bands, respectively. These values are in good agreement with the absolute intensities derived from CRDS experiments performed under very similar conditions, the only exception being that the temperature of the Np sample was slightly higher in the MICOS experiments (80 °C instead of 66 °C). This should have no or little effect, however, since all previous experiments show that there is an optimum sublimation temperature for Np around 70 °C beyond which point the number density of Np^+ tends to stabilize. The small, 7 ppm/pass, discrepancy found for the strongest band (40 ppm/pass in CRDS [7]) between the two sets of experiments can be easily accounted for

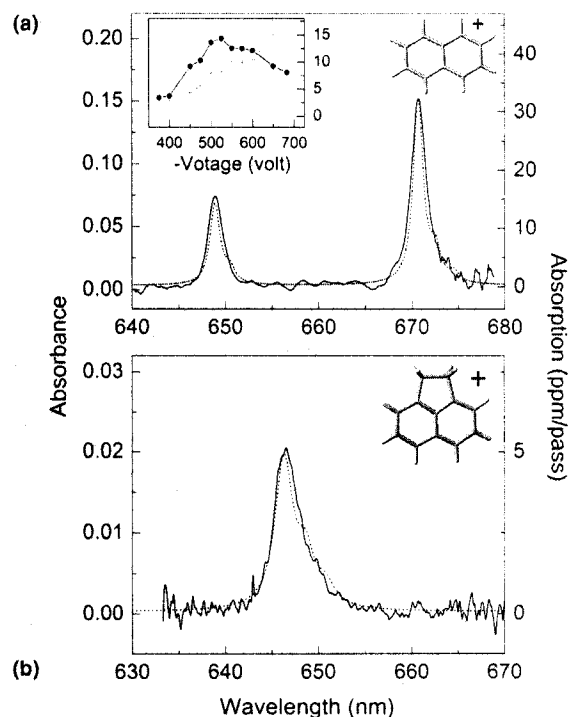


Fig. 3. Experimental and simulated MICOS spectra. (a) Spectrum of the (0–0) and (0–1) vibrational bands of the ${}^2B_{3g}(D_2) \leftarrow X^2A_u(D_0)$ electronic band system of the naphthalene cation ($C_{10}H_8^+$). Dotted line: synthetic spectrum corresponding to the spectrum of Np^+ , Np^+-Ar and Np^+-Ar_2 (in the 20:6:1 ratio derived from the CRDS spectra) convolved with the apparatus function of the spectrograph. Insert: Variation of the global extinction (dotted line) and of the absorption of the $D_2 \leftarrow D_0$ (1–0) band at 648.87 nm of the naphthalene cation (solid line) with the applied discharge voltage. (b) Spectrum of the (0–0) vibrational band of the $B_2(D_2) \leftarrow XA_2(D_0)$ electronic band system of the acenaphthene cation ($C_{12}H_{10}^+$). Dotted line: synthetic spectrum corresponding to the spectrum of Ac^+ , Ac^+-Ar and Ac^+-Ar_2 (in the 7.5:3:1 ratio derived from the CRDS spectra) convolved with the apparatus function of the spectrograph.

by the slight variability of the PDN source conditions from one experiment to another. The derived value for the relative intensity ratio of the two bands is 2.35 in MICOS measurements, in very good agreement with the value of 2.38 measured in previous experiments [6,9].

Taking advantage of the multiplex aspect of the MICOS spectrometer, we were also able to investigate the variation of the absorption intensity of Np^+ with the pressure of its neutral precursor (i.e., the dilution factor of Np in the carrier gas Ar) and with the discharge voltage applied to the PDN source. For instance, Insert of Fig. 3 shows that the Np^+ absorption signal (full line) reaches a maximum for a discharge voltage of about –550 V. The decrease observed for the signal from this point on is interpreted as due to the apparition of other formation/destruction channels for Np^+ . An increase of the global losses with the discharge voltage is also simultaneously observed and is attributed to the combination of two factors: an increase in the extinction

caused by the formation of carbon nanoparticles in the plasma (major factor) and the plasma-induced desorption of the molecular species that are adsorbed on the electrodes and the walls of the chamber and recondense on the mirrors (minor factor) [18,19].

3.2. The acenaphthene cation ($C_{12}H_{10}^+$)

Acenaphthene is a prototype for hydrogenated PAHs and it has been found in meteoritic samples [20]. Recent astrophysical models [21] predict that as much as 20% of the global PAH population found in the diffuse interstellar medium could be made of hydrogenated PAHs. Furthermore, recent laboratory studies show that the IR emission spectra of gas-phase hydrogenated PAHs [11] produce a good match to the satellite UIB bands in the 3.3–3.6 μm range while making little contribution to the other UIB bands. The MICOS spectrum of the $B_2(D_2) \leftarrow XA_2(D_0)$ (0–0) band of the acenaphthene cation (Ac^+) has been measured at 646.3 nm. The MICOS spectrum displayed in Fig. 3b is well reproduced by the convolution of the synthetic spectra of Ac^+ and the Ac^+-Ar and Ac^+-Ar_2 van der Waals (vdW) complexes with argon atoms (in the 7.5:3.0:1.0 intensity ratio derived from CRDS measurements [7]) with the apparatus function of the spectrometer. Following a similar approach as the one adopted for the naphthalene cation, absolute absorption intensities can also be derived for the acenaphthene cation. The conversion from the MICOS absorbance scale to an absorption scale yields a 4–5 ppm/pass peak maximum absorption. This value is consistent with the 7 ppm/pass peak absorption value measured with CRDS under similar experimental conditions [7]. Here too, the small difference found between the two sets of measurements can be attributed to the variability of the PDN source from one set of experiments to another.

3.3. The pyrene cation ($C_{16}H_{10}^+$)

Pyrene is a four benzenoid rings planar hydrocarbon. This molecule is considered as the prototype of compact PAH. Charged pyrene derivatives have been suggested as possible carriers for the strongest 4428 Å DIB [22]. This is the first time that the electronic absorption spectrum of the pyrene cation (and of a PAH ion as large as pyrene for that matter) is reported in the gas phase and the laboratory results will be discussed in detail in this case. Pyrene belongs to the D_{2h} symmetry group. In Fig. 4, we have adopted the geometry where the pyrene cation is oriented in the xy plane with the long axis in the x direction. In this section, we report and compare MICOS and CRDS measurements of the ${}^2B_{3g}(D_5) \leftarrow X^2A_u(D_0)$ vibrationless electronic band of the pyrene cation. Most of the analysis is based on the MICOS data.

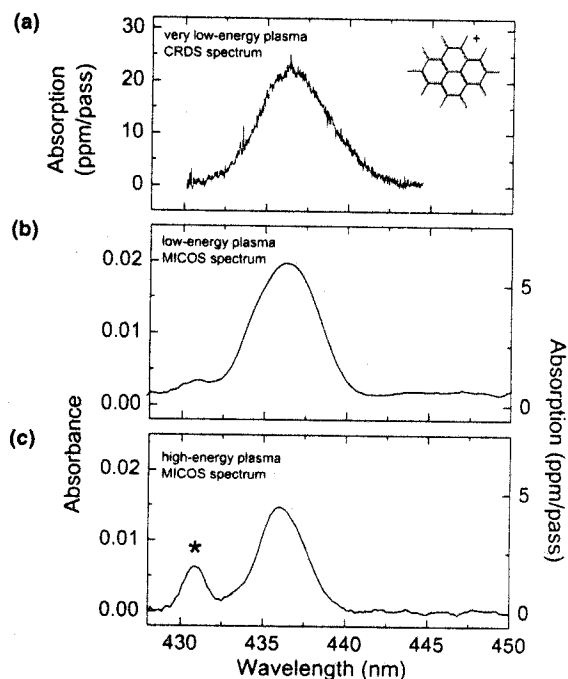


Fig. 4. (a) CRDS spectrum recorded at a backing pressure of 800 Torr and a discharge voltage of -450 V. (b) MICOS absorbance spectrum recorded at a discharge voltage of -500 V and a backing pressure of 906 Torr. (c) MICOS difference absorbance spectrum of the (0–0) vibrational band of the $D_5 \leftarrow D_0$ electronic band system of the pyrene cation ($C_{16}H_{10}^+$). The absorbance spectrum results from the subtraction of a medium energy plasma spectrum (-679 V) from a high-energy plasma spectrum (-780 V) both recorded at the same backing pressure of 761 Torr. The asterisk denotes the absorption of the CH radical.

The MICOS and CRDS absorption spectra of the discharge products formed in pyrene-seeded argon free jet expansions are shown in Fig. 4. Two bands are observed in the 425–465 nm spectral window. The strong absorption band centered around 436 nm is associated with the pyrene cation generated in the free jet and is discussed in detail below (see Sections 3.3.1 and 3.3.2). The weaker satellite band around 430.5 nm appears at ~ -550 V and its amplitude increases with the energy of the discharge. The variation of the relative intensities of the two bands clearly indicates that these two bands do not belong to the same molecular species. The weaker band is attributed to the (A–X) (0–0) absorption band of the CH radical formed by the fragmentation of the pyrene in the discharge [18].

3.3.1. The 436 nm band: analysis of the profile

The strongest feature that absorbs in the 436 nm range is assigned to the (0–0) vibrational band of the $D_5 \leftarrow D_0$ electronic band system of Py^+ (see Fig. 4). Determining accurate band peak position and bandwidth values for the free Py^+ requires taking into account the contribution of Py^+-Ar complexes formed in the jet to the profile of the measured band. It is a difficult task considering that the band has an extremely broad

profile. Based on previous spectroscopic studies on PAH⁺-Ar complexes [8,9,23], the vdW shift, δ , induced by the attachment of one argon atom to a PAH ion is expected to be less than 50 cm⁻¹. The full width at maximum of the 436 nm feature appears significantly larger than $n \times \delta$ (with $n = 1, 2$, is the number of Ar atoms attached to the Py⁺) making it difficult to extract the contribution of the complexes to the measured band envelope contrary to the cases of smaller size PAHs treated in our previous study [7]. The contribution of the complexes translates into a red-shift in the band peak position and a broadening of the band profile. The methodology we have adopted to solve this problem is to subtract a spectrum recorded at low plasma energy (in the -500 V range) from a set of spectra recorded at higher plasma energies (applied discharge voltage). The idea behind this procedure is that the increase in mean electron energy and electron number density (driven by the high voltage values) in the discharge should promote new paths of formation/destruction that enhance the [Py⁺]/[Py⁺-Ar_n] number density ratio. In particular, the probability of destruction of the weakly bound vdW complexes increases with the rate of collisions with high energy electrons.

Measurements performed at a fixed backing pressure of $p = 906$ Torr show that the band peak position shifts linearly to the blue (from 436.8 to 436.2 nm) when the magnitude of the applied discharge voltage varies from -550 to -850 V. The same measurements also show a reduction in the total bandwidth $\Delta\nu$, from 4.1 to 2.8 nm with the augmentation of the magnitude of the voltage (the band profile is fitted by a Lorentzian lineshape, after deconvolution with the apparatus function - $\delta\nu_{\text{app}} \sim 1$ nm). Based on the considerations detailed above, we adopt the value that is the most shifted to the blue, i.e. 436.2 ± 0.2 nm, for the band peak position and the smallest bandwidth i.e. 2.8 nm (or 145 cm⁻¹) as the intrinsic values for Py⁺. Having demonstrated in our previous experiments that the PAH cations formed through discharge are very efficiently cooled down in the supersonic expansion [7], we believe that the values obtained for the band profile and the bandwidth at high applied discharge voltage (i.e., high electron energy) are the closest to their intrinsic values.

The gas-phase position of the (0-0) D₅ ← D₀ absorption band of Py⁺ is shifted to the blue by 172 cm⁻¹ (0.76%) and 352 cm⁻¹ (1.56%) from its corresponding values in neon and argon solid matrices, respectively [22]. These shifts in energy are consistent with the values of 159 and 278 cm⁻¹ derived from photodepletion measurements of the D₄ ← D₀ (0-0) band at 480.3 nm [23].

The large bandwidth of 145 cm⁻¹ measured for the D₅ ← D₀ (0-0) transition cannot be accounted for by vibrational heating or by unresolved rotational structure as we discussed previously [7]. It is, instead, character-

istic of an ultra-fast relaxation mechanism that is associated with internal electronic conversion (IC) followed by intramolecular vibrational redistribution (IVR). This mechanism has already been observed for several PAH cations [7-9,24]. In the frame of the statistical limit of the radiationless transitions theory, the value of the relaxation time (~ 36 fs) depends on the gap energy (2106 cm⁻¹) between the electronic level that is probed (D₅ here) and the closest level that lies below (D₄) [23]. Strictly speaking however, the statistical limit might not hold anymore in this case as the D₅ - D₄ gap energy is small. Other mechanisms of interactions might come into effect and explain the departure of the profile from a perfect Lorentzian bandshape. This might also explain why the bandwidth of the D₅ ← D₀ (0-0) transition is close to the one measured for the D₄ ← D₀ (0-0) transition [23] whereas the bandgap energy $\Delta E_{D_4-D_5} \sim 6800$ cm⁻¹ is more than three times larger than the one between D₄ and D₅. Finally, we note that the relaxation time is very close to the physical limit of 30 fs that corresponds to the *average* half-period of oscillation of the active vibrational modes (i.e. minimum time required to redistribute the energy stored in a vibrational mode).

A 16:1 maximum absorbance ratio between the D₅ ← D₀ (0-0) 436.2 nm and the D₄ ← D₀ (0-0) 480.3 nm bands is found in Matrix Isolation Spectroscopy (MIS) measurements. An absorption cross section value of $\sigma = 1.6 \times 10^{-16}$ cm² for the 436.2 nm band can be extrapolated from the value measured by photodepletion for the 480.3 nm band. It translates into a $\alpha/\sigma \sim 4.4 \times 10^9$ /cm³ pyrene ion number density for a 7 ppm/pass absorption. With a dilution factor of pyrene in argon of the order of 1.7×10^{-3} (the vapor pressure of pyrene is ~ 1.3 Torr at a reservoir temperature of 160 °C [25]), and a number density of Ar of 5×10^{17} /cm³ in the probing zone 3.5 mm downstream the nozzle (as derived from flow simulations [26]), the ionization yield ζ is estimated to be about 5×10^{-6} , a value very close to the equivalent value of 1×10^{-5} derived for the naphthalene cation [7].

3.3.2. Comparison of MICOS and CRDS data

The electronic spectrum of the pyrene ion was also recorded with CRDS. A typical CRDS spectrum measured at low discharge voltage (-450 V) and at moderate generation pressure (~ 800 Torr) is reported in Fig. 4 where it is compared to MICOS spectra measured at both low and high discharge energy. The CRDS spectrum shows a 21 ppm/pass maximum absorption band with a 4.2 nm bandwidth. There is good agreement between the MICOS and CRDS band profiles recorded at low voltage. Absolute absorption values vary, however, between CRDS and MICOS spectra that were measured under slightly different backing pressures (800 and 906 Torr, respectively) and discharge voltages (-450 and

–500 V, respectively) all other parameters being equal (dilution, time-window probe). MICOS spectra recorded at –500 V typically show a 0.02 peak absorbance that is equivalent to a 7 ppm/pass absorption. In this particular case, the differences in the experimental conditions may well be the main cause of the discrepancy in absolute absorption values. As noted above, the slightly varying running conditions of the PDN source from one experiment to the other might impact the dynamical behavior of the plasma and might also contribute to this difference (e.g., the variation of the amount of soot deposited on the electrodes affects the electronic energy of the discharge).

4. Conclusion

A new variant of the ICOS technique, Multiplex ICOS (MICOS), has been developed, coupled to a pulsed discharge nozzle, and applied, for the first time, to the measurement of the gas-phase spectrum of large aromatic cations (up to 16 carbon atom PAHs) and to the detection of small carbon nanoparticles. The main conclusions that can be derived from this study and from a comparison with CRDS data are that:

- MICOS can achieve detection limits close to pulsed CRDS. MICOS however presents the additional, main advantage of multiplexity. In particular, MICOS allows real-time optimization of the absorption signal (1 s) and reduces dramatically the acquisition time (down to 30 s).
- MICOS is suitable for the investigation of broad spectral features and is thus particularly well adapted to the study of large carbon-bearing molecules and ions in the gas-phase. Higher fluxes might be needed in the case of weak narrow lines that require the use of a high-resolution spectrograph (i.e., small entrance slit width and high dispersion).
- The successful operation of MICOS demonstrates that it is possible to use a broadband dye laser source for the injection of photons into the optical cavity.
- The first measurement of the vibronic spectrum of the pyrene cation in the gas phase is reported. A procedure has been developed to retrieve the intrinsic profile for the $D_5 - D_0$ (0–0) vibronic band of Pyrene⁺ ($C_{16}H_{10}^+$). The band peaks at 436.2 nm with a FWHM of 2.8 nm (145 cm^{-1}). The broadening of the spectrum that is not accounted for by vibrational heating or rotational structure is due to internal electronic conversion followed by intramolecular vibrational redistribution as it has been shown for the naphthalene and acenaphthene cations. Py⁺ initially excited in the D_5 electronic level relaxes on an ultrafast timescale (~ 36 fs).
- We also identify CH as one of the high-energy plasma fragmentation products formed in the PDN through

the measurement of the CH (A–X) (0–0) absorption band. The yield of the CH fragmentation channel of pyrene is one order of magnitude higher than the ionization yield under high-energy conditions making the CH radical absorption a potential probe of the plasma.

- Finally, the plasma induced formation of carbon nanoparticles is observed for the first time – to our best knowledge – in a PDN source. This preliminary finding holds some potential for exploring the formation (and destruction) processes of carbon bearing molecules in astrophysically relevant environments (i.e., low temperature, non-collisional interstellar environments) and will be discussed in detail in an upcoming Letter [18].

Acknowledgements

This work is supported by the NASA Office of Space Science/Space Astrophysics Research and Analysis Program (RTOP # 188-01-00-21). A. O'Keefe and M. Gupta acknowledge support from the NASA SBIR Project NAS2-99045. L. Biennier is a National Research Council Associate at NASA-Ames Research Center. The authors wish to acknowledge R. Walker for outstanding technical support. We also thank Thomas Pino and Philippe Bréchnignac for providing their data on the $D_4 \leftarrow D_0$ band of the pyrene cation before publication.

References

- [1] K. Sellgren, *Spectrochim. Acta A* 57 (2001) 627.
- [2] G.P. van der Zwet, L.J. Allamandola, *Astron. Astrophys.* 146 (1985) 76.
- [3] A. Léger, L.B. D'Hendecourt, *Astron. Astrophys.* 146 (1985) 81.
- [4] F. Salama, E. Bakes, L.J. Allamandola, A.G.G.M. Tielens, *Astrophys. J.* 458 (1996) 621.
- [5] F. Salama, *Solid Interstellar Matter: The ISO Revolution*, EDP Sciences, France, 1999, p. 65.
- [6] D. Romanini, L. Biennier, F. Salama, A. Kachanov, L.J. Allamandola, F. Stoeckel, *Chem. Phys. Lett* 303 (1999) 165.
- [7] L. Biennier, F. Salama, L.J. Allamandola, J.J. Scherer, *J. Chem. Phys.* 118 (2003) 7863.
- [8] P. Bréchnignac, T. Pino, *Astron. Astrophys.* 343 (1999) 49.
- [9] T. Pino, N. Boudin, P. Bréchnignac, *J. Chem. Phys.* 111 (1999) 7337.
- [10] J. Oomens, A.G.G.M. Tielens, B.G. Sartakov, G. von Helden, G. Meijer, *Astrophys. J.* 591 (2003) 968.
- [11] D.R. Wagner, H.S. Kim, R.J. Saykally, *Astrophys. J.* 545 (2000) 854.
- [12] A. O'Keefe, *Chem. Phys. Lett.* 293 (1998) 331.
- [13] R. Engeln, G. Berden, R. Peeters, G. Meijer, *Rev. Sci. Instrum.* 69 (1998) 3763.
- [14] T. Gherman, D. Romanini, *Opt. Express* 10 (2002) 1033.
- [15] S.E. Fiedler, A. Hese, A.A. Ruth, *Chem. Phys. Lett.* 371 (2003) 284.
- [16] J.J. Scherer, J.B. Paul, H. Jiao, A. O'Keefe, *Appl. Opt.* 40(2001)6725.
- [17] K. Liu, R.S. Fellers, M.R. Viant, R.P. McLaughlin, M. Brown, R. Saykally, *Rev. Sci. Instrum.* 67 (1996) 410.
- [18] L. Biennier, F. Salama, in preparation.

- [19] F. Grangeon, C. Monard, J.L. Dorier, A.A. Howling, C. Hollenstein, D. Romanini, N. Sadeghi, *Plasma Sources Sci. Technol.* 8 (1999) 448.
- [20] A. Shimoyama, *Adv. Space. Res.* 19 (1997) 1045.
- [21] V. Le Page, Y. Keheyani, T.P. Snow, V.M. Bierbaum, *Int. J. Mass. Spectrom.* 185/186/187 (1999) 949.
- [22] F. Salama, L.J. Allamandola, *Nature* 358 (1992) 42.
- [23] T. Pino, Ph.D. thesis, Université d'Orsay, Paris, France, 1999.
- [24] P. Bréchignac, T. Pino, N. Boudin, *Spectrochim. Acta A* 57 (2001) 745.
- [25] K. Nass, D. Lenoir, A. Kettrup, *Angew. Chem. Int. Ed. Engl.* 34 (1995) 1735.
- [26] A. Benidar, L. Biennier, F. Salama, in preparation.